Revisiting the NIR-to-Visible Upconversion Mechanism in beta-NaYF4:Yb3+,Er3+

ARTICLE *in* JOURNAL OF PHYSICAL CHEMISTRY LETTERS · DECEMBER 2013

Impact Factor: 7.46 · DOI: 10.1021/jz402366r

4 AUTHORS, INCLUDING:

Steve J. Smith
South Dakota School of Mines and Technology
68 PUBLICATIONS **791** CITATIONS
SEE PROFILE

Stanley May
University of South Dakota
81 PUBLICATIONS **1,227** CITATIONS
SEE PROFILE

Berry Mary
University of South Dakota
61 PUBLICATIONS **1,203** CITATIONS
SEE PROFILE

THE JOURNAL OF PHYSICAL CHEMISTRY Letters

Letter

pubs.acs.org/JPCL

Revisiting the NIR-to-Visible Upconversion Mechanism in β-$NaYF_4$:Yb^{3+},Er^{3+}

Robert B. Anderson,[†] Steve J. Smith,[†] P. Stanley May,[‡] and Mary T. Berry*[,‡]

[†]Nanoscience and Nanoengineering, South Dakota School of Mines and Technology, 501 East Saint Joseph Street, Rapid City, South Dakota 57701, United States

[‡]Department of Chemistry, University of South Dakota, 414 East Clark Street, Vermillion, South Dakota 57069, United States

Supporting Information

ABSTRACT: Here, we show that the long-accepted mechanism for the production of red and blue emission through upconversion (UC) of 1 μm excitation in Yb^{3+}/Er^{3+}-doped materials does not apply in the popular β-$NaYF_4$ host. We propose a new mechanism involving Yb^{3+}-to-Er^{3+} energy-transfer UC out of the green-emitting $^2H_{11/2}$,$^4S_{3/2}$ states that quantitatively accounts for all of the observed optical behavior. Rate constants for the relevant radiative and nonradiative processes are reported along with a prediction of the power dependence of the pulsed and continuous-wave UC quantum efficiency.

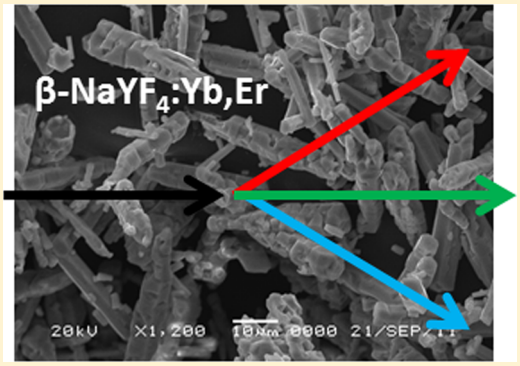

SECTION: Plasmonics, Optical Materials, and Hard Matter

As far back as 1966, Auzel described how energy-transfer upconversion (ETU) could lead to visible emission following NIR excitation of f elements doped in an inorganic host.[1] Since that time, physically plausible ETU mechanisms for the production of red, green, and blue upconversion (UC) emission from the Yb^{3+}/Er^{3+} donor/acceptor couple have been proposed and are summarized in a 2004 review[2] as well as other seminal papers.[3] Here, we show that the long-accepted mechanism for the production of red and blue emission through UC of 1 μm excitation in Yb^{3+}/Er^{3+}-doped materials does not apply in the popular β-$NaYF_4$ host. We propose a new mechanism that quantitatively accounts for all of the observed optical behavior. Furthermore, we show how this mechanism strongly limits the quantum efficiency (QE) of the green emission.

Interest in lanthanide-based UC phosphors has burgeoned since the development of synthetic methods[4] for creating highly processable nanomaterials with applications in biolabeling,[5,6] sub-band gap energy harvesting in photovoltaics,[7,8] and security printing.[9] Much basic research has been performed in order to understand the origin of the relatively high UC efficiencies,[10] the ability to tune the color purity through manipulating dopant concentrations,[11] and the special phenomenona that result from surface effects in nanoscale UC phosphors.[12,13]

β-$NaYF_4$:Yb^{3+},Er^{3+} has been reported as the most efficient UC material with measured QEs for production of green luminescence from 1 μm excitation on the order of 3% at an excitation flux of 20 W/cm^2.[14,15] At this excitation flux, the efficiency of the red luminescence approaches that of the green, and the blue luminescence efficiency also becomes significant. The main features of the standard, currently accepted mechanism for production of red, green, and blue UC are illustrated in the left-hand panel of Figure 1. In this mechanism, green luminescence arises from the $^2H_{11/2}$,$^4S_{3/2}$ levels via a two-photon process with sequential energy transfer wherein the Er^{3+} is excited first from $^4I_{15/2}$ to $^4I_{11/2}$ and, subsequently, from $^4I_{11/2}$ to $^4F_{7/2}$, which relaxes nonradiatively to the thermalized emitting-state manifold, $^2H_{11/2}$,$^4S_{3/2}$. Red emission arises from $^4F_{9/2}$ after $^4S_{3/2}$ decays nonradiatively to $^4F_{9/2}$ or when ETU promotes Er^{3+} from $^4I_{13/2}$ to $^4F_{9/2}$. The requisite $^4I_{13/2}$ is populated by well-established Er−Er cross relaxation, which is also illustrated in the diagram. These processes account for the observation that although the power dependence of the green emission suggests a two-photon process, the red emission shows a power dependence implicating contribution from a three-photon process. Blue UC emission from $^2H_{9/2}$ has also been observed[16] and attributed to ETU promoting Er^{3+} from $^4F_{9/2}$ up to, or just above, the blue-emitting $^2H_{9/2}$.

It was our intention to quantitatively determine values for the microscopic rate constants for energy transfer, radiative relaxation, and so forth, by creating a large set of optical data and modeling the optical behavior with coupled rate equations describing the changing populations of the Er^{3+} and Yb^{3+} energy levels. In this model, the rate constants were treated

Received: November 3, 2013
Accepted: December 3, 2013
Published: December 3, 2013

   dx.doi.org/10.1021/jz402366r | J. Phys. Chem. Lett. 2014, 5, 36−42

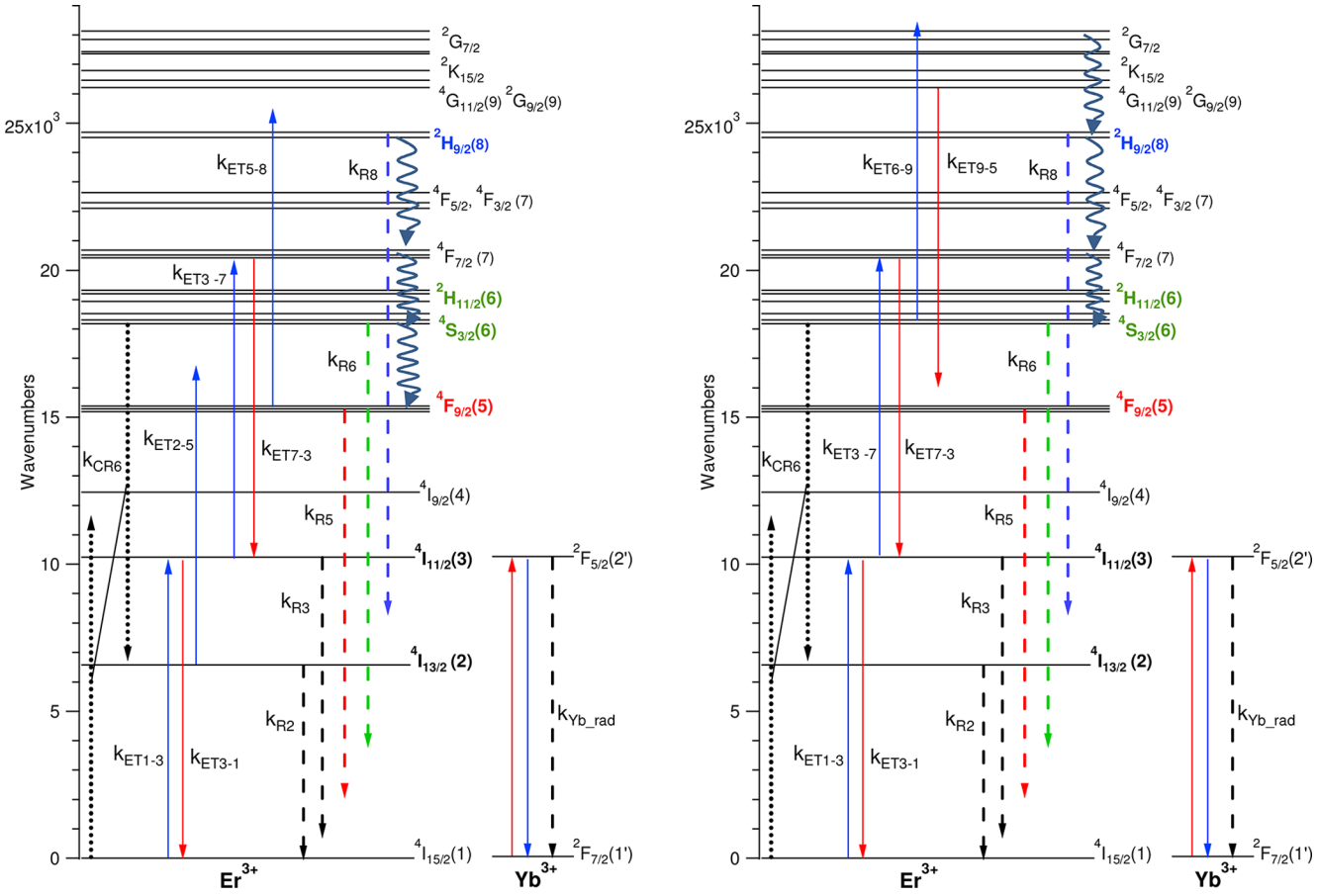

Figure 1. Energy level diagram illustrating the essential steps in the standard (left panel) and new (right panel) ETU mechanisms. The k_{ETx-y} represent rate constants for Yb−Er energy transfer, in both forward and back directions. The k_{Rx} are rate constants for radiative relaxation out of level x, k_{CR} is the rate constant for Er−Er cross relaxation, and k_{Yb_rad} is the rate constant for radiative relaxation from Yb^{3+} ($^2F_{5/2}$). To maintain simplicity, multiphonon relaxation from the excited levels is illustrated with unlabeled curvy arrows. The fundamental difference in the two models is inclusion of ETU into and out of the ^2K,^4G manifold in the new model.

as free parameters, adjusted to give the best fit between model predictions and measured optical behavior.

Using micrometer-sized powders of β-$NaYF_4$:18%Yb^{3+},2% Er^{3+}, we measured luminescence decay curves following pulsed excitation at 943 nm for the blue, green, red, and 1 and 1.5 μm emission over a range of excitation fluxes from 2 to 200 mJ/cm^2 per pulse. We measured the emission spectra under those same conditions in order to assess the relative intensities of the emission features as well as their power dependence. We also measured down-conversion phenomena, decay curves, and relative intensities, following excitation directly above the emitting levels of interest. The standard UC model produced a very poor fit, especially with regard to the green-to-red intensity ratio and with regard to the time dependence of the red and blue UC luminescence. Looking for alternate or additional steps in the mechanism, we noted that the shape of the blue UC curve (i.e., time dependence following pulsed NIR excitation) is closely matched by a multiplicative product of the green curve and the 1 μm curve. This strongly implies that the major source of the blue UC at these power densities is ETU from $^4S_{3/2}$ (the green-emitting state) and not from $^4F_{9/2}$ (the red-emitting state). A comparison of the blue, green, and 1 μm decay curve shapes is illustrated in the left panel of Figure 2, and the relevant new ETU step is illustrated in the right-hand panel of Figure 1 with an arrow labeled k_{ET6-9}. We further note that this ETU process involves initial excitation into the ^4G,^2K manifold, above $^2H_{9/2}$, with subsequent nonradiative relaxation down to the $^2H_{9/2}$ blue-emitting state. If we excite directly into this ^4G,^2K manifold, it is clear that there is also a rapid process that populates the red-emitting state, $^4F_{9/2}$ from ^4G,^2K. This is illustrated in the lower right-hand panel of Figure 2, where, with direct excitation into ^4G,^2K at 375 nm, we see an instantaneous rise on the red emission, similar to the rise time on the blue emission from $^2H_{9/2}$, suggesting that they are both fed from ^4G,^2K. In contrast, the rise on the green emission is much slower, similar to the fall time on the blue and consistent with nonradiative relaxation from $^2H_{9/2}$ to $^2H_{11/2}$,$^4S_{3/2}$. Furthermore, the green-to-red intensity ratio following excitation into ^4G,^2K is 0.39, whereas excitation just above the green-emitting states produces a green-to-red ratio of 20. Clearly, exciting at $^4G_{11/2}$ or above provides an efficient path to $^4F_{9/2}$, the red-emitting state. We attribute this path to back energy transfer to Yb^{3+}, as illustrated in the right-hand panel of Figure 1 (labeled k_{ET9-5}) as opposed to a new Er−Er cross relaxation. Er−Er cross relaxation is eliminated because we have observed that the green-to-red intensity ratio shows little dependence on the Er^{3+} concentration, whereas Er−Er cross relaxation would be suppressed at lower concentrations (see the Supporting Information).

The 1 μm curve after excitation at 375 nm shows two components in the rise time. There is an instantaneous component, consistent with the back energy transfer that also produced red

dx.doi.org/10.1021/jz402366r | J. Phys. Chem. Lett. 2014, 5, 36−42

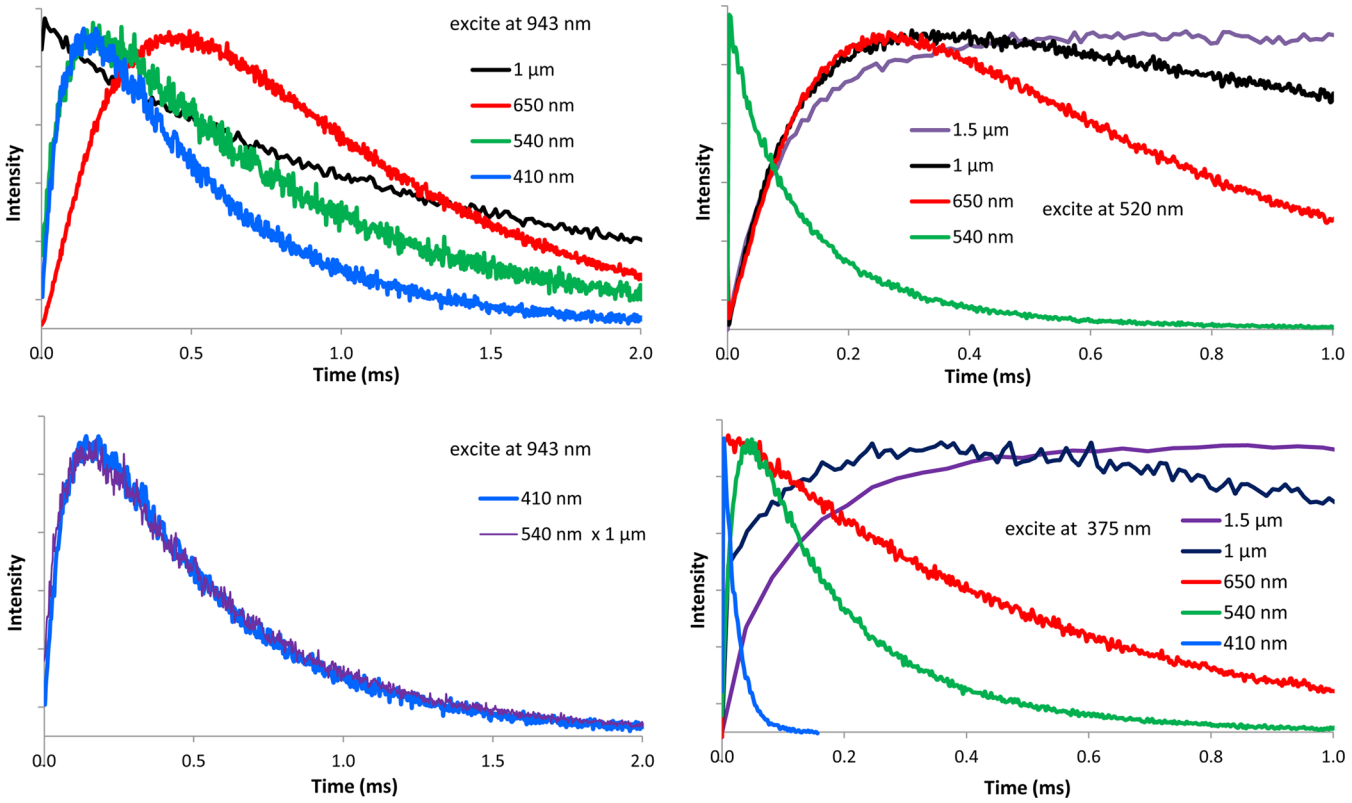

Figure 2. The two left-hand panels illustrate the UC luminescence decay curves following pulsed excitation at 943 nm. The shape of the curve for blue emission (410 nm) is very closely matched by the multiplicative product of the green emission curve (540 nm) and the 1 μm emission, suggesting that the blue arises from ETU out of the green ($^4S_{3/2}$) state. The right-hand panels show the down-conversion emission decay curves following pulsed excitation at 520 and 375 nm. Both the blue (410 nm) and the red (650 nm) curves show a nearly instantaneous rise upon excitation at 375 nm, which may be contrasted with the relatively slow rise on the red following excitation at 520 nm. All of the curves are normalized to a similar maximum intensity in order to compare shapes as opposed to brightness.

emission, and a slower component, matching the fall time of the green emission and consistent with cross relaxation out of green state that results in population of the 1 and 1.5 μm emitting states.

Thus, we propose that there are two new processes, labeled with k_{ET6-9} and k_{ET9-5} in the right-hand panel of Figure 1, that should be included in the model. Including these new processes resulted in an excellent fit to experimental data, alleviating the poor agreement between the experiment and model in the green-to-red intensity ratio and bringing the decay curve shapes into much better agreement. A comparison of the two models for the red and blue curves and for the green-to-red intensity ratio is shown in Figure 3. The best-fit parameters (rate constants) for both the standard model and the new model are given in Table 1. The new model suggests that nonradiative relaxation out of the green state makes very little contribution to the red UC emission and that the ETU rate constant, k_{ET2-5}, predicted to directly feed red emission in the standard model, is nearly zero. Practically all of the red emission arises from back energy transfer to Yb^{3+} accompanied by Er^{3+} relaxation from $^4G_{11/2}$ down to $^4F_{9/2}$. Neither of the mechanistic steps for population of $^4F_{9/2}$ from the standard UC model makes a significant contribution. Interestingly, this implies that red emission is excited almost exclusively via a three-photon process, whereas the higher-lying green-emitting state is populated via a two-photon process.

The new UC model may be used to predict QEs for both pulsed and cw experiments as illustrated in Figure 4. In both cases, the green QE shows a maximum of 3−4%, falling off as the red and blue intensities continue to grow with power. The position of the maximum in the green QE for the CW prediction is in very good agreement with Page,[15] who found a maximum QE of 2% at 20W/cm^2 for a mixed-phase powder sample of $NaYF_4$:18%Yb,2%Er. Van Veggel made a quantum yield measurement for micrometer-sized powders of the pure β-phase $NaYF_4$:20%Yb,2%Er, finding QE = 3.0 ± 0.3% at 20 W/cm^2, in close agreement with our predictions.[14] Our calculations suggest that the observed fall off in the green QE after reaching a maximum at 20 W/cm^2 is a result of ETU out of $^4S_{3/2}$, which pumps the states that produce red and blue emission.

Thus, by simply adding the experimentally verified ETU step from $^4S_{3/2}$ up to the $^4G,^2K$ manifold (see k_{ET6-9} in Figure 1) and by including the clearly evident Er-to-Yb back energy transfer with Er relaxing from $^4G_{11/2}$ to $^4F_{9/2}$ (see k_{ET9-5} in Figure 1), we are able to reproduce all of the power-dependent luminescence decay curve shapes and all of the power-dependent intensity ratios observed in experiment. The model also correctly predicts the QE behavior. Furthermore, the fit creates a set of quantitative values for rate constants that may be used in further prediction and critical tests of the model. In particular, we intend to apply the new model to nanomaterials, where surface quenching will impact multiphonon relaxation rates. As other examples, the model may be used to predict QEs as a function of dopant concentration or to determine which specific rate constants are impacted through interaction with

dx.doi.org/10.1021/jz402366r | J. Phys. Chem. Lett. 2014, 5, 36−42

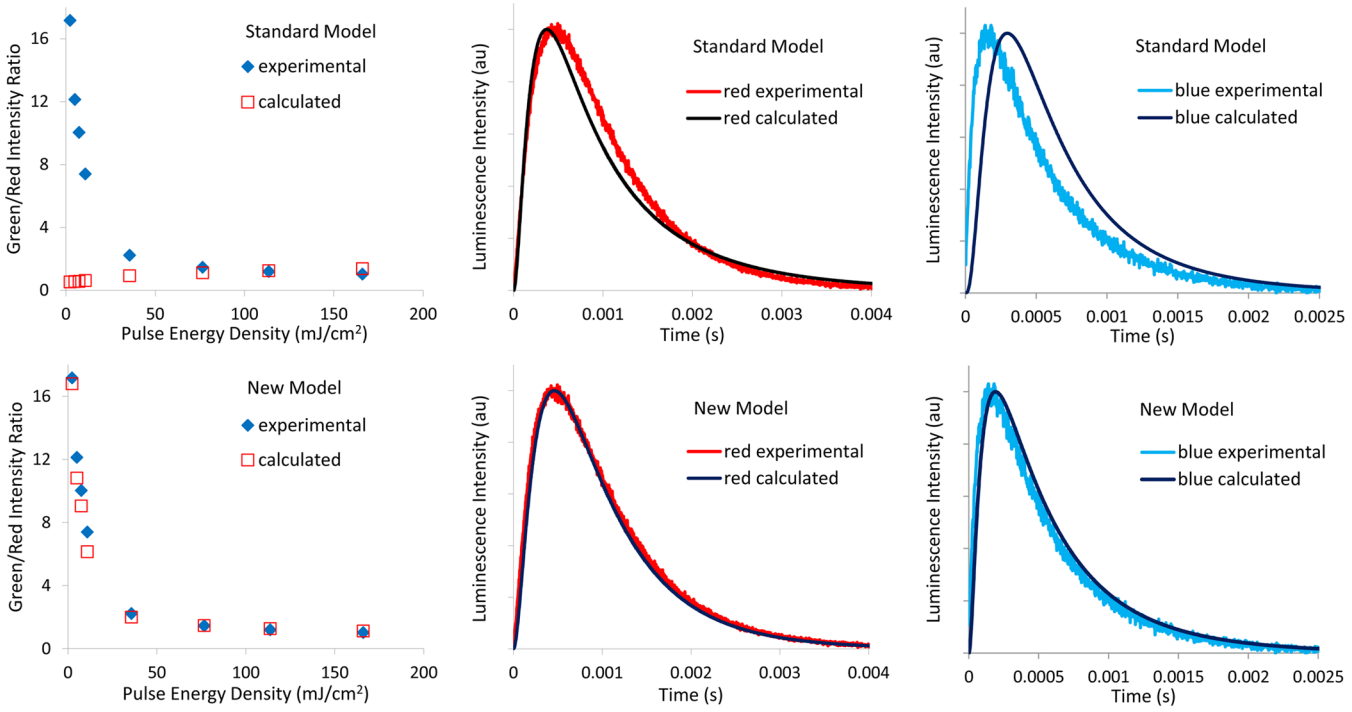

Figure 3. The new UC model corrects the error in the power dependence of the green-to-red intensity ratio and improves the match of the experimental versus calculated curve shapes. For the standard model, a parameter set can be found with a better match than that shown above for the green-to-red intensity ratio, but this creates a much worse fit in the curve shapes, such that the overall error in the fit is increased. The excitation pulse energy density for the red and blue luminescence decay curves was 66 mJ/cm^2/pulse.

plasmonic surfaces. The new UC model with quantitative values for the rate constants will provide a powerful tool for either predicting or correctly interpreting the optical properties of the most widely studied UC phosphor.

EXPERIMENTAL METHODS

Sample. Phase-pure β-$NaYF_4$/18%Yb^{3+},2%Er^{3+} was obtained from Lorad Chemical Corporation. The material was a pinkish-white powder with micrometer-sized, rod-shaped crystallites as determined by SEM. The phase purity was assessed with powder XRD (see the Supporting Information).

Spectroscopy. For UC experiments, excitation at 943 nm was provided by a dye laser (Continuum ND 6000) pumped by a pulsed Nd:YAG laser (Continuum Surelite II). The dye used was LDS 925 (Exciton). Excitation was set at 943 nm, rather than at the maximum absorbance near 980 nm, in order to allow collection of emission at 980 nm without interference from laser scatter. Excitation for down-conversion experiments was provided by an optical parametric oscillator (Optotek, Inc., Opolette) or by a dye laser pumped by a nitrogen laser (Laser Photonics DL-14/UV-14). Emission was collected by a 0.3 m monochromator (TRIAX 320, Horiba) and detected with a photomultiplier tube (Hamamatsu R2658P, R5108, or H10330A-75) using photon counting (SR430 multichannel scaler, SRS). The PMT signal was preamplified (SR 445A, SRS) prior to photon counting.

Modeling. The set of coupled rate equations as given below was developed to reflect the time-dependent changes in populations of the Yb and Er energy levels.

For Yb^{3+}:

$$\dot{n}_2' = F\sigma n_1' - k_{Yb}n_2' - k_{ET1-3}n_1n_2' - k_{ET2-5}n_2n_2' - k_{ET3-7}n_3n_2' - k_{ET5-8}n_5n_2' - k_{ET6-9}n_6n_2' + k_{ET3-1}n_3n_1' + k_{ET7-3}n_7n_1' + k_{ET9-5}n_9n_1'$$

$$\dot{n}_1' = -\dot{n}_2'$$

For Er^{3+}:

$$\dot{n}_9 = k_{ET6-9}n_6n_2' - k_{ET9-5}n_9n_1' - k_{NR9}n_9$$

$$\dot{n}_8 = k_{ET5-8}n_5n_2' + k_{NR9}n_9 - k_{NR8}n_8 - k_{R8}n_8$$

$$\dot{n}_7 = k_{NR8}n_8 + k_{ET3-7}n_3n_2' - k_{ET7-3}n_7n_1' - k_{NR7}n_7$$

$$\dot{n}_6 = k_{NR7}n_7 - k_{ET6-9}n_6n_2' - k_{NR6}n_6 - k_{R6}n_6 - k_{CR6}n_6n_1$$

$$\dot{n}_5 = k_{NR6}n_6 + k_{ET2-5}n_2n_2' + 0.04k_{R8}n_8 - k_{ET5-8}n_5n_2' + k_{ET9-5}n_9n_1' - (k_{NR5} + k_{R5})n_5$$

$$\dot{n}_4 = k_{NR5}n_5 + k_{UC2}n_2n_2 - k_{CR4}n_4n_1 - k_{NR4}n_4$$

$$\dot{n}_3 = k_{NR4}n_4 + k_{ET1-3}n_1n_2' + k_{ET7-3}n_7n_1' + k_{CR6}n_6n_1 + 0.05k_{R5}n_5 + 0.05k_{R6}n_6 + 0.14k_{R8}n_8 - k_{ET3-1}n_3n_1' - (k_{NR3} + k_{R3})n_3 - k_{ET3-7}n_3n_2'$$

$$\dot{n}_2 = k_{NR3}n_3 + 0.19k_{R3}n_3 + 0.05k_{R5}n_5 + 0.25k_{R6}n_6 + 0.42k_{R8}n_8 + k_{CR6}n_6n_1 + 2k_{CR4}n_4n_1 - 2k_{UC2}n_2n_2 - k_{R2}n_2 - k_{ET2-5}n_2n_2'$$

dx.doi.org/10.1021/jz402366r | J. Phys. Chem. Lett. 2014, 5, 36−42

Table 1. Best-Fit Parameters for the Standard and New UC Models[a]

Lorad μm-sized powders			
parameter	standard UC model	new UC model	±standard deviation
	Yb Parameters (s^{-1})		
k_{Yb}	645	613	±83
k_{Yb_rad}	429	393	±54
	Yb-to-Er Energy Transfer Parameters (cm^{-3} s^{-1})		
k_{ET1-3}/k_{ET3-1}	7.9	5.9	±2.5
k_{ET2-5}	0.00×10^{-15}	0.00×10^{-15}	$\pm 0.00 \times 10^{-15}$
k_{ET3-7}	2.64×10^{-15}	1.54×10^{-15}	$\pm 0.14 \times 10^{-15}$
k_{ET5-8}	9.44×10^{-15}	1.76×10^{-15}	$\pm 0.26 \times 10^{-15}$
k_{ET6-9}	n/a	6.07×10^{-15}	$\pm 0.85 \times 10^{-15}$
	Er-to-Yb Back Transfer Parameters (cm^{-3} s^{-1})		
k_{ET3-1}	$[2 \times 10^{-16}]$	$[2 \times 10^{-16}]$	n/a
k_{ET5-2}	0.00×10^{-16}	0.00×10^{-16}	$\pm 0.00 \times 10^{-16}$
k_{ET7-3}	2.17×10^{-16}	2.04×10^{-16}	$\pm 0.17 \times 10^{-16}$
k_{ET9-5}	n/a	2.84×10^{-16}	$\pm 0.79 \times 10^{-16}$
	Nonradiative Relaxation Parameters (s^{-1})		
k_{NR9}	2.20×10^{6}	1.76×10^{6}	$\pm 0.43 \times 10^{6}$
k_{NR8}	45 200	43 450	±190
k_{NR7}	$[1.0 \times 10^{6}]$	$[1.0 \times 10^{6}]$	n/a
k_{NR6}	1892	26	±3
k_{NR5}	0.0	0.0	±0.0
k_{NR4}	25 400	22 120	±550
k_{NR3}	32	61	±17
	Radiative Decay Parameters (s^{-1})		
k_{R8} (blue, 410 nm)	1490	2330	±200
k_{R6} (green)	880	1510	±38
k_{R5} (red)	2770	2039	±24
k_{R3} (1 μm)	130	73	±18
k_{R2} (1.5 μm)	111	110	±1
	Er−Er Cross-Relaxation Parameters (cm^{-3} s^{-1})		
k_{CR6}	2.48×10^{-17}	2.79×10^{-17}	$\pm 0.06 \times 10^{-17}$
k_{CR4}	1.53×10^{-18}	8.04×10^{-19}	$\pm 0.44 \times 10^{-19}$
	Additional Parameters		
k_{UC2} (cm^{-3} s^{-1})	1.92×10^{-17}	2.31×10^{-17}	$\pm 0.21 \times 10^{-17}$
β (fraction of isolated Yb^{3+} and Er^{3+})	0.16	0.05	±0.01
	Errors in Least-Squares Fit		
error	7.5%	3.1%	
intensity ratios	38.%	9.6%	
curves (average)	5.1%	2.7%	
blue curves	8.9%	3.4%	
green curves	3.6%	2.9%	
red curves	7.8%	2.9%	
1 μm curves	2.6%	2.2%	
1.5 μm curves	2.4%	2.4%	
no. of intensity ratios in fit	32	32	
no. of curves in fit	43	43	

[a]The new UC model gives a much better fit to the intensity ratios (err = 10 versus 38%) and a much better fit to the decay curve shapes, especially for the red (err = 3 versus 8%) and blue curves (err = 3 versus 9%). The parameter values for the new UC model are the average values from 20 fits with randomly chosen starting points. The last column gives the sample standard deviation from those 20 fits.

$$\dot{n}_1 = k_{R2}n_2 + 0.81k_{R3}n_3 + 0.90k_{R5}n_5 + 0.70k_{R6}n_6 + 0.40k_{R8}n_8 - k_{CR6}n_6n_1 - k_{CR4}n_4n_1 + k_{UC2}n_2n_2 - k_{ET1-3}n_1n_2' + k_{ET3-1}n_3n_1'$$

In these equations, n_x refers to the population of level x where $x = 1-9$, as indicated in Figure 1. The k_{Rx} and k_{NRx} refer to radiative and multiphonon relaxation rate constants from level x. The k_{ETx-y} are Yb^{3+}/Er^{3+} energy-transfer rate constants, where x and y refer to the initial and final Er^{3+} states, respectively. The parameter k_{CRx} is the rate constant for cross relaxation from Er^{3+} level x. The parameter $k_{Yb} = k_{Yb\_rad} + k_{Yb\text{-}NR}$ is the intrinsic rate constant for decay of the excited state $Yb^{3+}(^2F_{5/2})$. The parameter F represents the photon flux for CW excitation, and σ is the absorbance cross section. The parameter, k_{UC2} represents the rate constant for the process in which two adjacent Er^{3+}, both excited to $^4I_{13/2}$, may undergo ETU and result in one excited Er^{3+} at $^4I_{11/2}$ and a second in the ground state, $^4I_{15/2}$. The emission branching ratios, represented by the premultipliers of the radiative rate constants, were measured from emission

dx.doi.org/10.1021/jz402366r | J. Phys. Chem. Lett. 2014, 5, 36−42

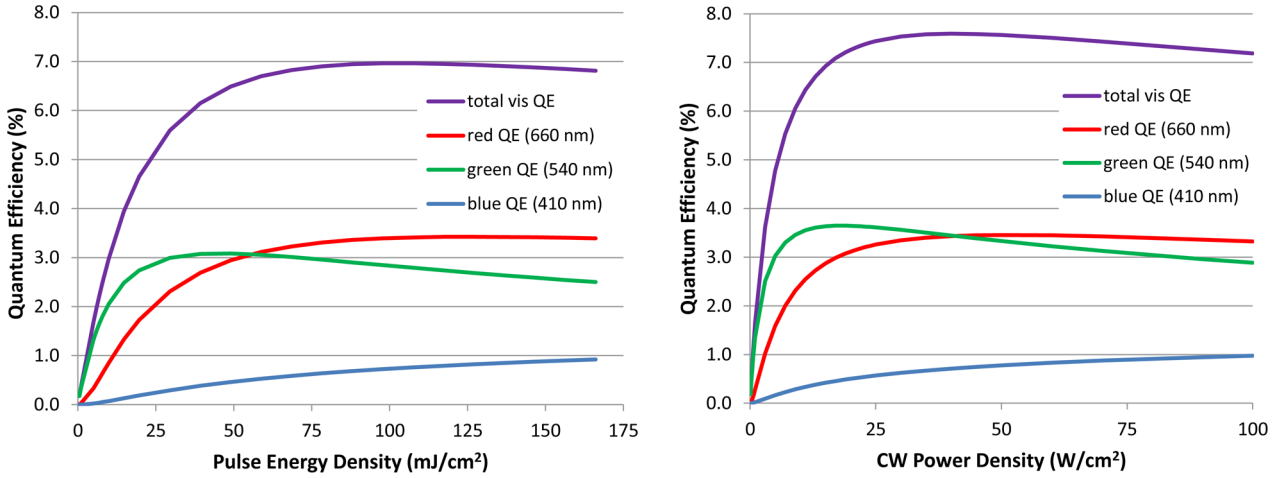

Figure 4. Power dependence of the calculated QEs under pulsed and CW excitation at 980 nm. In both cases, the fall off in the green QE results from the ETU process that pumps population out of the green-emitting state and into the blue and red.

spectra and calculated from Judd−Ofelt parameters. They are similar to the branching ratios reported by Feng et al. for Er^{3+} doped in oxyfluoride glass.[17]

A fraction of the Er^{3+} and Yb^{3+} ions in the matrix might be expected to be isolated from other Er^{3+} or Yb^{3+} ions and therefore not participate in ETU or cross relaxation. The parameter β, which appears as the value 0.05 in Table 1, represents that fraction.

The rate equations were solved simultaneously using the Euler method with a time step of 640 ns. The time-dependent populations, $n_x(t)$ were used to calculate luminescence decay curve shapes and relative intensities. These were compared to experimentally determined curve shapes and intensities, allowing the rate constants to vary as free parameters, chosen to provide the minimum least-squares deviation between calculated and experimentally determined quantities. In order to evaluate the precision in determination of the parameters, a process of simulated annealing was performed. A random number generator was used to vary the starting parameter set for a new fit, each parameter varied within ±60% of a previously determined best-fit value. Forty such fits were run, with 20 converging to an error similar to the previously determined best fit. The parameters reported in Table 1 are the average values from the 20 fits along with the sample standard deviation.

■ ASSOCIATED CONTENT

Ⓢ Supporting Information

A scanning electron micrograph and powder XRD of the sample are given. Also given is a diffuse reflectance spectrum, a comparison between measured and calculated power dependence in the UC luminescence, and a table of Er^{3+} concentration dependence of the green-to-red intensity ratio. An Er^{3+}/Yb^{3+} energy level diagram, illustrating all of the two-ion interactions, supplements the interactions illustrated in Figure 1. This material is available free of charge via the Internet at http://pubs.acs.org.

■ AUTHOR INFORMATION

Corresponding Author

*E-mail: mary.berry@usd.edu.

Notes

The authors declare no competing financial interest.

■ ACKNOWLEDGMENTS

The authors acknowledge support from NSF (EPS-0903804 & DGE-0903685) and the State of South Dakota, Governor's Office of Economic Development. P.S.M. acknowledges support from NASA (Cooperative Agreement Number: NNX10AN34A). Computational resources of USD High Performance Computing facilities maintained by Doug Jennewein are gratefully acknowledged

■ REFERENCES

(1) Auzel, F. Compteur Quantique par Transfert d'Energie Entre de Yb^{3+} a Tm^{3+} dans un Tungstate Mixte et dans Verre Germinate. *C. R. Acad. Sci. (Paris)* **1966**, *263*, 819−821.

(2) Auzel, F. Upconversion and Anti-Stokes Processes with f and d Ions in Solids. *Chem. Rev.* **2004**, *104*, 139−174.

(3) Suyver, J. F.; Grimm, J.; Krämer, K. W.; Güdel, H. U. Highly Efficient Near-Infrared to Visible Up-Conversion Process in $NaYF_4$:Er^{3+},Yb^{3+}. *J. Lumin.* **2005**, *114*, 53−59.

(4) Heer, S.; Kömpe, K.; Güdel, H.-U.; Haase, M. Highly Efficient Multicolour Upconversion Emission in Transparent Colloids of Lanthanide-Doped $NaYF_4$ Nanocrystals. *Adv. Mater.* **2004**, *16*, 2102−2105.

(5) Chen, J.; Guo, C.; Wang, M.; Huang, L.; Wang, L.; Mi, C.; Li, J.; Fang, X.; Mao, C.; Xu, S. Controllable Synthesis of $NaYF_4$:Yb, Er Upconversion Nanophosphors and Their Application to *In Vivo* Imaging of *Caenorhabditis elegans*. *J. Mater. Chem.* **2011**, *21*, 2632−2638.

(6) Wang, F.; Banerjee, D.; Liu, Y.; Chen, X.; Liu, X. Upconversion Nanoparticles in Biological Labeling, Imaging, and Therapy. *Analyst* **2010**, *135*, 1839−1854.

(7) van Sark, W. G. J. H. M.; de Wild, J.; Rath, J. K.; Meijerink, A.; Schropp, R. E. I. Upconversion in Solar Cells. *Nanoscale Res. Lett.* **2013**, *8*, 81−89.

(8) Zou, W.; Visser, C.; Maduro, J. A.; Pshenichnikov, M. S.; Hummelen, J. C. Broadband Dye-Sensitized Upconversion of Near-Infrared Light. *Nat. Photonics* **2012**, *6*, 560−564.

(9) Meruga, J. M.; Cross, W. M.; May, P. S.; Luu, Q.; Crawford, G. A.; Kellar, J. J. Security Printing of Covert Quick Response Codes Using Upconverting Nanoparticle Inks. *Nanotechnology* **2012**, *23*, 395201.

(10) Renero-Lecuna, C.; Martín-Rodríguez, R.; Valiente, R.; González, J.; Rodríguez, F.; Krämer, K. W.; Güdel, H. U. Origin of the High Upconversion Green Luminescence Efficiency in β-$NaYF_4$:2%Er^{3+},20%Yb^{3+}. *Chem. Mater.* **2011**, *23*, 3442−3448.

(11) Chan, E. M.; Han, G.; Goldberg, J. D.; Gargas, D. J.; Ostrowski, A. D.; Schuck, P. J.; Cohen, B. E.; Milliron, D. J. Combinatorial

Discovery of Lanthanide-Doped Nanocrystals with Spectrally Pure Upconverted Emission. *Nano Lett.* **2012**, *12*, 3839−3845.
(12) Wang, F.; Wang, J.; Liu, X. Direct Evidence of a Surface Quenching Effect on Size-Dependent Luminescence of Upconversion Nanoparticles. *Angew. Chem., Int. Ed.* **2010**, *49*, 7456−7460.
(13) Zhao, J.; Lu, Z.; Yin, Y.; McRae, C.; Piper, J. A.; Dawes, J. M.; Jin, D.; Goldys, E. M. Upconversion Luminescence with a Tunable Lifetime in $NaYF_4$ Nanocrystals: Role of Nanocrystal Size. *Nanoscale* **2013**, *5*, 944−952.
(14) Boyer, J.-C.; van Veggel, F. C. J. M. Absolute Quantum Yield Measurements of Colloidal $NaYF_4$: Er^{3+}, Yb^{3+} Upconverting Nanoparticles. *Nanoscale* **2010**, *2*, 1417−1419.
(15) Page, R. H; Schaffers, K. I.; Waide, P. A.; Tassano, J. B.; Payne, S. A.; Krupke, W. F.; Bische, W. K. Upconversion-Pumped Luminescence Efficiency of Rare-Earth-Doped Hosts Sensitized with Trivalent Ytterbium. *J. Opt. Soc. Am. B* **1998**, *15*, 996−1008.
(16) Suyver, J. F.; Grimm, J.; van Veen, M. K.; Biner, D.; Krämer, K. W.; Güdel, H. U. Upconversion Spectroscopy and Properties of $NaYF_4$ Doped with Er^{3+}, Tm^{3+}, and/or Yb^{3+}. *J. Lumin.* **2006**, *117*, 1−12.
(17) Feng, L.; Wang, J.; Tang, Q.; Hu, H.; Liang, H.; Su, Q. Optical Properties of Er^{3+}-Singly Doped and Er^{3+}/Yb^{3+}-Codoped Novel Oxyfluoride Glasses. *J. Non-Cryst. Solids* **2006**, *352*, 2090−2095.